Photodissociation of O_3 around 309 nm

Nori Taniguchi, Kenshi Takahashi, and Yutaka Matsumi*

Solar-Terrestrial Environment Laboratory and Graduate School of Science, Nagoya University, Honohara 3−13, Toyokawa, Aichi, 442-8507, Japan

Received: May 5, 2000; In Final Form: July 20, 2000

Photodissociation reaction of O_3 following ultraviolet photon excitation around the thermodynamic threshold of the dissociation channel of $O(^1D) + O_2(a^1\Delta_g)$ at 309.44 nm has been studied under room-temperature and jet-cooled conditions. Both $O(^1D)$ and $O(^3P)$ photoproducts are detected by a technique of vacuum ultraviolet laser-induced fluorescence (VUV-LIF) spectroscopy. Photofragment excitation (PHOFEX) spectra for the $O(^1D)$ and $O(^3P)$ atoms are obtained by scanning the photolysis laser wavelength between 297 and 316 nm while monitoring VUV-LIF signal intensities at 115 and 130 nm for $O(^1D)$ and $O(^3P)$, respectively. From the behavior of the PHOFEX spectra for the $O(^3P)$ and $O(^1D)$ atoms around the threshold into $O(^1D) + O_2(a^1\Delta_g)$, the existence of an exit barrier along the $O-O_2$ dissociation coordinate in the photoexcited electronic state of O_3 is suggested. Analysis of the line widths in the jet-cooled PHOFEX spectra of $O(^1D)$ and $O(^3P)$ suggests that the quasi-bound states below the barrier and above the threshold have lifetimes of 0.2−0.8 ps. The $O(^1D)$ quantum yield values from the O_3 photolysis are obtained from the PHOFEX spectrum for $O(^3P)$ at 295 K. The $O(^1D)$ quantum yields between 297 and 305 nm are almost independent of the photolysis wavelength ($\approx$0.89), which is smaller than the current NASA/JPL recommendation for atmospheric modeling (0.95). The physical model for $O(^1D)$ formation in the photolysis of O_3 in the wavelength range 305−329 nm is presented, which can quantitatively explain the temperature and wavelength dependence of $O(^1D)$ quantum yield.

Introduction

The photodissociation reaction of O_3 following photoexcitation by solar ultraviolet (UV) radiation plays a key role in atmospheric chemistry and its importance has motivated a lot of experimental and theoretical studies.[1−3] Photoabsorption of O_3 in the ultraviolet region consists of two bands:[4−7] the wide bell-shaped absorption peaked at around 250 nm is called Hartley band, while a vibrational structure in the long wavelength edge of Hartley band in the 310−360 nm region is called Huggins band. Figure 1 shows a schematic diagram of the intersections for the O_3 potential energy surfaces (PESs) as a function of the bond length for one of the O−O bonds. The Hartley band is attributed to the transitions onto the saddle-geometry region of the electronically excited $^1B_2$ PES corresponding to ground-state equilibrium configurations with strong Franck−Condon (FC) overlap (Figure 1).[8] The origin of the Huggins band has been the subject of controversial discussions and there are two explanations. One is that the Huggins band structure is attributed to the transitions to some bound states on the excited $^1B_2$ PES displaying small FC overlaps with the ground state, so that the Huggins band comes from the same transition as the Hartley band.[9−11] The other is the transition to the 2^1A_1 PES, and small cross sections are due to its orbitally forbidden character[12−15] The potentical curve for the 2^1A_1 state is not depicted in Figure 1.

The UV ozone photolysis in the wavelength region around 300−330 nm can proceed via five energetically allowed channels:[1−3]

$$O_3 + h\nu\ (\lambda < 309\ \text{nm}) \rightarrow O(^1D) + O_2(a^1\Delta_g) \quad (1)$$

$$O_3 + h\nu\ (\lambda < 1180\ \text{nm}) \rightarrow O(^3P) + O_2(X^3\Sigma_g^-) \quad (2)$$

$$O_3 + h\nu\ (\lambda < 411\ \text{nm}) \rightarrow O(^1D) + O_2(X^3\Sigma_g^-) \quad (3)$$

$$O_3 + h\nu\ (\lambda < 463\ \text{nm}) \rightarrow O(^3P) + O_2(b^1\Sigma_g^+) \quad (4)$$

$$O_3 + h\nu\ (\lambda < 612\ \text{nm}) \rightarrow O(^3P) + O_2(a^1\Delta_g) \quad (5)$$

where wavelengths given in parentheses indicate the thermodynamic cutoff for each channel. Recent experimental studies[15−25] confirmed that not only the spin-allowed channels (1) and (2) which are predominant in the Hartley band but also spin-forbidden channels (3)−(5) occur in the Huggins band. When ozone is photoexcited in the Hartley band at $\lambda < 309$ nm, the excited state ($^1B_2$) gives rise to channel (1) dissociation, while the potential crossing between the $^1B_2$ and R states leads to channel (2) dissociation (see Figure 1). The experimental studies[15,21] at wavelengths longer than about 320 nm suggested that the channel (3) products are formed as a result of the crossing of the singlet exit channel (R state), which leads to the channel (2) products, by triplet states correlating with the channel (3) products. Theoretical studies about the O_3 triplet states correlating to the spin-forbidden products (3)−(5) have not been carried out. The inferred triplet state which is responsible for the channel (3) products is schematically depicted by a broken curve in Figure 1.

Among the photoproducts from the UV photolysis of O_3, the $O(^1D)$ atom plays active and ubiquitous roles in the photochemical processes of the Earth's atmosphere.[1,2] Much attention has been paid into the wavelength and temperature dependence of the quantum yield of the $O(^1D)$ formation from the O_3

* Electronic mail: matsumi@stelab.nagoya-u.ac.jp. Fax: + 81-533-89-5593.

10.1021/jp001706i CCC: $19.00
Published on Web 09/13/2000

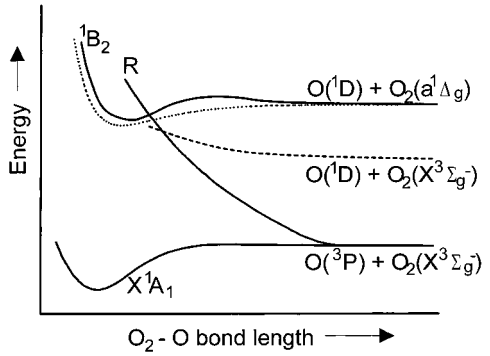

Figure 1. Schematic section through the approximate low-lying potential energy surfaces (PESs) of O_3 along a dissociation coordinate $R(O_2-O)$. The potential curve diagram presented by Hay et al.[8] is modified. A broken curve is added as the potential curve representing the triplet state which is responsible for the spin-forbidden formation of $O(^1D)$. A dotted curve is also added for the $O(^1D) + O_2(^1\Delta_g)$ formation without an exit energy barrier (see text). Symmetry representations are shown in the C_{2v} point group.

photolysis at around 315 nm, since it is very important to evaluate the oxidative capacity in the troposphere and lower stratosphere. Numerous previous studies indicated that channel (1) is predominant at wavelengths $\lambda < 306$ nm and the $O(^1D)$ quantum yield is almost independent of the photolysis wavelength, with a reported quantum yield of 0.9−0.95 throughout the Hartley band.[3] For $\lambda > 306$ nm, the $O(^1D)$ quantum yield decreases sharply with increasing the photolysis wavelength λ,[16,18,20−23] since the energetic threshold for channel (1) lies at 309.44 ± 0.03 nm.[26] Even below the energetic threshold into channel (1), the $O(^1D)$ quantum yield does not simply reach to zero. This is because there are other processes to produce $O(^1D)$ atoms even at $\lambda > 309.44$ nm. Between 309 and ca. 320 nm, the $O(^1D)$ atoms arise predominantly from the photodissociation of vibrationally excited O_3 molecules which are thermally populated under atmospheric conditions. Takahashi et al.[15] pointed out that prior excitation in the asymmetric stretching (ν_3) vibration extensively promotes the photoabsorption, which results in the fragmentation into $O(^1D) + O_2(a^1\Delta_g)$ through channel (1). The high effectiveness of the ν_3 mode in the hot band excitation was explained by the large enhancement of the Franck−Condon factors between the photoexcited $^1B_2$ state and the ν_3 excited levels in the ground electronic state. Theoretical calculations on the O_3 PESs indicate that the energetically minimum point in the ground electronic state is located at an equal length position for the two O−O bonds, while the $^1B_2$ photoexcited state has minimum points at unequal length positions.[8,10,12,13] In the wavelength region of $\lambda >$ ca. 320 nm, the formation of $O(^1D)$ does not result predominantly from the hot band excitation but from the spin-forbidden dissociation channel (3).[15−23] Although the quantum yield of $O(^1D)$ from channel (3) is small (≈0.06−0.08),[20−23] its contribution has a great impact on the $O(^1D)$ production rate in atmospheric chemistry.[22,23]

On the basis of the laboratory studies on the O_3 photolysis in the near UV region, mathematical expressions for the $O(^1D)$ quantum yield as functions of photolysis wavelength and temperature have been proposed for application to atmospheric modeling. The NASA/JPL recommendation[27] adopted the formulation presented by Michelsen et al.[28] Recent experimental studies have verified that the NASA/JPL recommendation underestimates the atmospheric $O(^1D)$ production yield, especially at the longer photolysis wavelengths ($\lambda > 320$ nm). The discrepancy is attributable to contribution from the $O(^1D)$ atoms generated via the spin-forbidden channel (2), which is not included in the current NASA/JPL recommendation. Talukdar et al.[22] suggested a model to calculate the $O(^1D)$ yield, $\Phi(\lambda,T)$ at wavelength λ and at temperature T, using an analytical function:

$$\Phi(\lambda,T) = 0.06 + A_\lambda \exp\left(-\frac{B_\lambda}{T}\right) \quad (6)$$

where A_λ and B_λ are the wavelength-dependent constants. In eq 6 the offset of 0.06 corresponds to the contribution of the spin-forbidden channel (3), which is not included in the NASA/JPL formulation.[27]

In this paper, we report experimental studies on the formation processes of $O(^3P)$ and $O(^1D)$ atoms from photolysis of O_3 around 309 nm under room-temperature and jet-cooled conditions. The PHOFEX spectra are measured by scanning the photolysis laser wavelength while monitoring VUV-LIF intensities at 115 and 130 nm for $O(^1D)$ and $O(^3P_j)$, respectively. The existence of an exit barrier along the $O-O_2$ bond breaking direction on the PES of the photoexcited $^1B_2$ state of O_3 is suggested from the analysis of the PHOFEX spectra near the thermodynamic threshold for channel (1) at 309.44 nm. The $O(^1D)$ quantum yields in the wavelength range 296−312 nm are obtained from the room-temperature PHOFEX spectrum for $O(^3P)$. A new numerical model to explain the mechanism and the quantum yield values for $O(^1D)$ formation from the photolysis of O_3 in the wavelength range 305−329 nm has been presented.

Experimental Section

The experimental apparatus used to study ozone photochemistry in our laboratory has been described in detail elsewhere[16] and we give only brief description pertinent to the current study here. O_3 was prepared by passing ultrapure O_2 (Nihon Sanso, 99.9995%) through a commercial ozonizer and collected on silica gel at a liquid nitrogen/methanol slush temperature (ca. 175 K). Once sufficient O_3 was produced, residual gas was pumped away and the ozone desorbed into a blackened storage glass bulb. Ozone photolysis was performed (a) under conditions of substantial cooling in a pulsed expansion and (b) under flow conditions at room temperature (295 K). In the supersonic jet experiments, a gas mixture (typically 2−3% O_3 in He, at a total pressure of ca. 1000 Torr, 1 Torr = 133.3 Pa) was injected through a pulsed nozzle (General Valve, Series 9, hole diameter 0.8 mm) into the stainless steel vacuum chamber, evacuated by a liquid-nitrogen trapped oil diffusion pump. During the experiments, typical background pressure in the vacuum chamber was 1×10^{-4} Torr when the pulsed nozzle was operated at a repetition rate of 10 Hz with a duration of 230 μs. In the flow cell experiments, a mixture of O_3 (1%) in Helium gases was slowly flowed into a photodissociation cell which was pumped by a rotary pump (330 L/min) through a liquid nitrogen trap. The total pressure in the flow cell was maintained at 1 Torr.

The O_3 molecules were photolyzed by the tunable laser light in the wavelength range 297−316 nm, which was generated by a Nd:YAG pumped dye laser (Lambda Physik, Scanmate 2EC-400) with a second harmonics generation crystal (KD*P). The typical photolysis laser pulse energies were 0.5 mJ. The wavelength of the fundamental visible light was calibrated by simultaneously measuring the laser-induced fluorescence excitation spectrum of iodine vapor and comparing it with published chart.[29]

The $O(^3P_j)$ photofragments from O_3 were detected by VUV-LIF method for the $3s\ ^3S°-2p\ ^3P_j$ transition at 130.22 nm for

$j = 2$, 130.48 nm for $j = 1$, and 130.60 nm for $j = 0$. The VUV laser around 130 nm was generated by four-wave difference mixing ($2\omega_1 - \omega_2$) in krypton gas,[30] using two dye lasers simultaneously pumped by a XeCl excimer laser (Lambda Physik FL3002's and Lextra-50). Typical pressure of the Kr gas in the mixing cell was 15 Torr. The dye laser output (Bis-MSB laser dye in 1,4-dioxane) was frequency-doubled by a BBO crystal for ω_1 wavelength of 212.56 nm, which was two-photon resonant with Kr $5p[^1/_2]_0$. The wavelength of ω_2 (Coumarin 540A in methanol) was around 578.1, 572.8, and 570.6 nm for $j = 2$, 1, and 0, respectively.

For the detection of the O(^{1}D) photofragments from O_3 photolysis, the probe laser system was rearranged to observe the VUV-LIF of the 3s ^{1}D°−2p ^{1}D transition at 115.22 nm. The 115.22 nm laser light was generated by phase-matched frequency tripling of the output from a dye laser at 345.6 nm in Xe (40 Torr)/Ar (120 Torr) gas mixture.[31] The dye laser pumped by the XeCl excimer laser was used with PTP dye solution to generate the 345.6 nm light (∼5 mJ/pulse incident laser intensity). The laser beam(s) for the four-wave mixing or the frequency tripling were focused with a lens ($f = 200$ mm) into the Kr or Xe/Ar containing cell. The generated VUV laser light was introduced into the reaction chamber through a LiF window. The bandwidth of the 115 nm VUV radiation was estimated to be 0.65 cm^{-1} (fwhm).

The photolysis and probe laser pulses were counterpropagated and separated in time by 100 ns using a pulse delay controller (Stanford Research, DG535). The VUV-LIF signals associated with both the O(^{1}D) and the O(^{3}P) photoproducts were detected along the vertical direction, orthogonal to propagation direction of both VUV probe and photolysis laser beams, using a solar-blind photomultiplier tube (EMR, 541J-08−17). The output from the photomultiplier was recorded using a boxcar (Stanford Research, SR-250) and stored on a pc. The signal intensity in the PHOFEX spectra was corrected to the intensity of the VUV laser by recording the photoionization current from a sample of NO contained (typically 2 Torr) within a cell with lithium fluoride window located after the main a vacuum chamber.

Results

Figure 2 shows the photofragment excitation (PHOFEX) spectrum for O(^{3}P) atoms produced in the photodissociation of O_3 under room-temperature conditions (295 K). For measurements of the PHOFEX spectrum, the wavelength of the VUV probe laser was fixed to the center of the 3s ^{3}S°−2p $^3P_2$ resonance line at 130.22 nm for O($^3P_2$), while the wavelength of the UV photolysis laser was continuously scanned between 297 and 314 nm. Two factors should be considered to verify that the obtained PHOFEX spectrum for O($^3P_2$) is proportional to the total O(^3P_j, j=0, 1 and 2) yield in the photolysis of O_3: one is the Doppler profiles of O(^3P_j) fragments and the other is the fine structure branching ratio (j-distribution) among the spin-orbit levels of the O(^3P_j) fragments. The line width of the VUV probe laser light (∼0.83 cm^{-1}) is narrower than the Doppler spectral width of the nascent O(^3P_j) fragments. If the Doppler width of the nascent O(^3P_j) were strongly dependent on the photolysis wavelength, the PHOFEX spectrum might not be proportional to the O(^3P_j) yield spectrum. The width of the O(^3P_j) Doppler line shapes was found to be independent of the photolysis wavelength and remained almost constant value (1.05 cm^{-1}). No obvious variation in line width was discernible over the photolysis wavelength range 297−314 nm. This is reasonable because the spin-allowed dissociation process of channel (2) is predominant and the O(^{3}P) formation via the spin-forbidden channels (4) and (5) is very small in this wavelength range. We also measured the branching ratios among the j-levels of the O(^3P_j) atoms produced from the O_3 photolysis at several photolysis wavelengths. The results obtained for the j-branching are listed in Table 1. The j-branching remained almost constant in the wavelength range 297−316 nm, and were in good agreement with the previous reports.[16,21,32] Thus, these measurements confirmed that the PHOFEX spectrum for the O($^3P_2$) fragments in Figure 2 is proportional to the total yield spectrum for O(^3P_j).

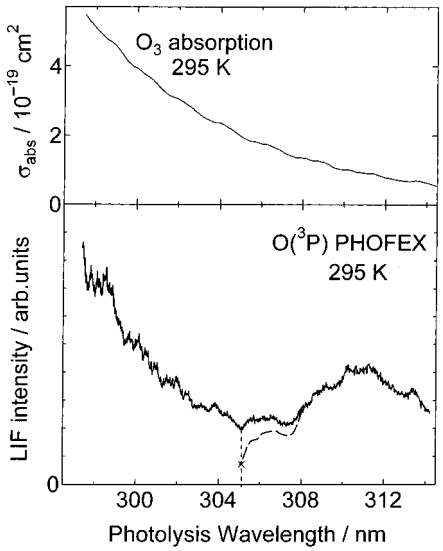

Figure 2. Photofragment excitation (PHOFEX) spectrum for O(^{3}P) atoms produced from the photolysis of O_3 taken under flow conditions at 295 K. The PHOFEX spectrum was obtained by scanning the photolysis laser wavelength between 297 and 314 nm while monitoring the VUV-LIF intensity of O(^{3}P) atoms at 130 nm. The PHOFEX spectrum was corrected for intensity variations of the photolysis and probe lasers. Photoabsorption spectrum of O_3 molecules at 295 K is also shown in the upper panel for comparison, which is reported by Malicet et al.[7] The broken curve in the lower panel represents the virtual PHOFEX spectrum for O(^{3}P) (see text).

TABLE 1: Fine Structure Branching Ratios for the Oxygen Atom O(^3P_j) from O_3 Photolysis at Various Photolysis Wavelengths

		population[c]		
λ[a]	T[b]	$j = 2$	$j = 1$	$j = 0$
297	295	0.64 ± 0.03	0.27 ± 0.02	0.09 ± 0.01
305	295	0.63 ± 0.02	0.28 ± 0.02	0.09 ± 0.01
310	295	0.63 ± 0.02	0.28 ± 0.02	0.09 ± 0.01
305[d]	227	0.60 ± 0.02	0.31 ± 0.02	0.10 ± 0.01
308[e]	295	0.65 ± 0.02	0.27 ± 0.02	0.08 ± 0.01
statistical[f]		0.56	0.33	0.11

[a] Photolysis wavelength in units of nm. [b] Sample gas temperature in units of K. [c] Normalized populations. [d] Reference 21. [e] Reference 16. [f] Degeneracy ratios, $2j + 1$.

Figure 3 shows the PHOFEX spectra for O(^{1}D) and O(^{3}P) fragments produced in the photodissociation of O_3 under jet-cooled and 295 K conditions. For measurements of the O(^{1}D) PHOFEX spectra, the wavelength of the VUV probe laser was fixed to the center of the 3s ^{1}D° − 2p ^{1}D resonance line at 115.22 nm for O(^{1}D), while the wavelength of the UV photolysis laser was continuously scanned. The invariance of the line widths of O(^{1}D) in the wavelength range of Figure 3 was also checked to ensure that the PHOFEX spectrum was proportional to the yield spectrum of O(^{1}D). The line width of the nascent O(^{1}D) fragments from O_3 photolysis at room temperature was also found to be independent of the photolysis wavelength (0.67

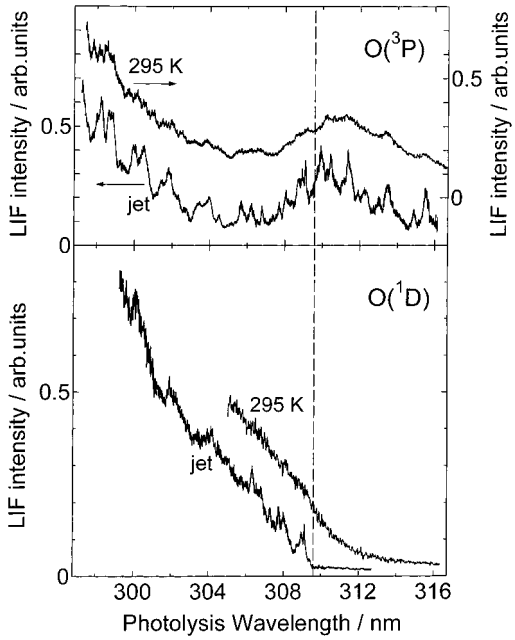

Figure 3. Comparison of photofragment excitation (PHOFEX) spectra taken under room temperature (295 K) and supersonic free-jet conditions for both $O(^1D)$ and $O(^3P)$ atoms produced from the photolysis of O_3. The PHOFEX spectra were obtained by scanning the photolysis laser wavelength while monitoring the LIF intensity of $O(^1D)$ or $O(^3P)$ atoms. Spectra were corrected for intensity variations of the photolysis and probe lasers. A vertical broken line indicates the thermodynamic threshold for the dissociation channel to $O(^1D) + O_2(^1\Delta_g)$ (=309.44 ± 0.03 nm).[26]

cm^{-1}). This implies that the $O(^1D)$ atoms probed are predominantly produced via channel (1), since O_3 is photolyzed around the channel (1) threshold and the resultant $O(^1D)$ fragments can have only a little translational energy. The PHOFEX spectra for $O(^1D)$ were corrected for photolysis and probe laser intensity variations. The linear dependence of the LIF signal on photolysis laser power at various photolysis wavelengths ensured that the $O(^1D)$ atoms come from one-photon dissociation of parent O_3. Thus, the $O(^1D)$ PHOFEX spectrum shown in Figure 3 can quantitatively reflect the relative yield of the $O(^1D)$ production.

The free-jet experiments were carried out with several different O_3/He mixing ratios in expansion gas (1−6%) and under different stagnation pressure conditions (700−1100 Torr). The PHOFEX spectra obtained were dependent neither on the O_3 concentration in the expansion gas nor on the stagnation pressure. This indicates that van der Waals complex or dimer molecules does not affect the PHOFEX spectra for $O(^1D)$ and $O(^3P)$ atoms. To estimate the rotational temperature of O_3 in the supersonic jets, the LIF spectrum of carbon monoxide (CO) was measured around 115 nm under the same jet conditions. The rotational lines associated with the (0,0) band of the electronic transition $B^1\Sigma^+ - X^1\Sigma^+$ [33] were recorded. Analysis of the spectra revealed that the rotational populations were well reproduced by a Boltzmann distribution at a rotational temperature of $T_{rot} = 3$ K. Similar rotational cooling should be achieved in the O_3 experiment.

As shown in Figure 3, the $O(^1D)$ yield in the supersonic beam decreases as the photolysis wavelength increases and a clear-cut-off for the $O(^1D)$ formation appears at 309.44 nm. The cutoff wavelength corresponds to an appearance potential of the dissociation path into $O(^1D) + O_2(a^1\Delta_g)$ (channel (1)) which is indicated by a broken line.[26] Accordingly the signal intensity of the $O(^1D)$ drastically changes at the threshold wavelength. A small amount of the $O(^1D)$ formation at $\lambda > 309.44$ nm is

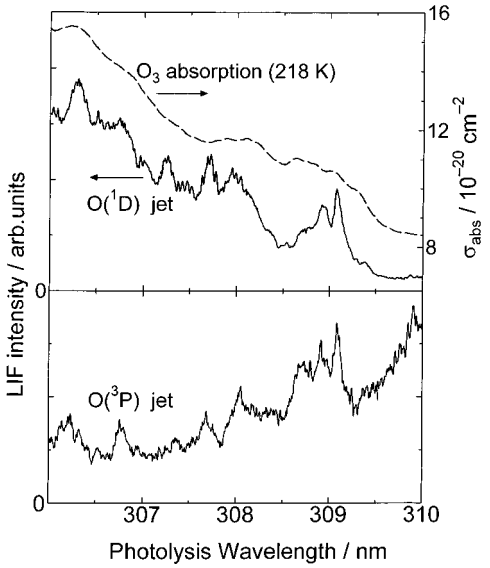

Figure 4. Detailed PHOFEX spectra of $O(^1D)$ and $O(^3P)$ atoms from the photolysis of O_3 under jet-cooled conditions in the wavelength range 306−310 nm. Spectra were corrected for the intensity variations of the photolysis and probe lasers.

attributed to the vibrationally hot-band excitation of the parent O_3 molecules. Under the supersonic free-jet conditions, the vibrational cooling of the parent molecules is less efficient than the rotational cooling.[34] On the other hand, such a cutoff is not clearly identified in the room-temperature PHOFEX spectrum for $O(^1D)$. This is due to contribution from the photolysis of rotationally excited O_3 in the thermal sample. As shown in the Figure 3, the spectral features are more resolved in the jet-cooled spectra than those at 295 K for both of the $O(^1D)$ and $O(^3P)$. These aspects indicate that the spectral broadening at 295 K is due to the overlaps of rotational envelopes among the vibrational bands.

Figure 4 shows the detailed PHOFEX spectra for $O(^1D)$ and $O(^3P)$ atoms between 306 and 310 nm taken under jet-cooled conditions. In both spectra, sharp peaks are discernible. The structures resemble to each other between the $O(^1D)$ and $O(^3P)$ spectra, although the contributions of the background continuum are different. The line widths of the sharp peaks are measured to be in the range 7−35 cm^{-1} in fwhm, which correspond to the lifetimes of 0.2−0.8 ps by the uncertainty principle. The photoabsorption spectrum for O_3 at 218 K [7] was also shown for comparison.

Figure 5 shows the quantum yield of $O(^1D)$ formation from the UV photolysis of O_3 at 295 K, as a function of the photolysis wavelength between 297 and 314 nm. The quantum yield spectrum for $O(^1D)$ production shown in Figure 5 is calculated by eq 7:

$$\Phi_{1D}(\lambda) \equiv \frac{\sigma_{1D}(\lambda)}{\sigma_{abs}(\lambda)} = 1 - \frac{\sigma_{3P}(\lambda)}{\sigma_{abs}(\lambda)} = 1 - \frac{s_{3P} Y_{3P}(\lambda)}{\sigma_{abs}(\lambda)} \quad (7)$$

where $\Phi_{1D}(\lambda)$ is the $O(^1D)$ quantum yield at a photolysis wavelength λ, $\sigma_{abs}(\lambda)$ is the total absorption cross section of O_3, $\sigma_{1D}(\lambda)$ and $\sigma_{3P}(\lambda)$ are the partial cross sections for $O(^1D)$ and $O(^3P)$ formation, respectively, and $Y_{3P}(\lambda)$ is the PHOFEX spectrum for $O(^3P)$ recorded at room temperature. s_{3P} represents the sensitivity factor in the $O(^3P)$ detection. In the wavelength range shown in Figure 5, only the two states of O atoms can be produced from the photolysis of O_3, that is, $\sigma_{abs}(\lambda) = \sigma_{1D}(\lambda) + \sigma_{3P}(\lambda)$. The absorption cross sections of O_3 reported by Malicet

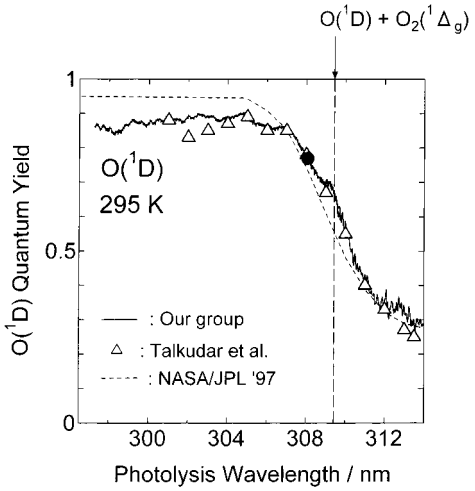

Figure 5. Quantum yields of the $O(^1D)$ formation from the ultraviolet photolysis of O_3 at room temperature (295 K) as a function of the photolysis wavelength. The $O(^1D)$ quantum yields are obtained from the $O(^3P)$ PHOFEX spectrum in Figure 2, using eq 7 obtained in this study for 297−314 nm (see text). The dot curve shows the NASA/JPL recommendation[27] for use in the stratospheric modeling. Open triangles indicate the recent experimental results by Talukdar et al.[22] The filled circle at 308 nm indicates the reference value point (=0.79). A vertial broken line indicates the thermochemical threshold for channel of $O(^1D) + O_2(^1\Delta_g)$.

TABLE 2: $O(^1D)$ Quantum Yields from the Photolysis of O_3 in the Wavelength Range 295−308 nm at 295 K

λ (nm)[a]	this work[b]	Talukdar et al.[c]	NASA/JPL[d]
295		0.91 ± 0.01	0.95
297	0.89 ± 0.02		0.95
298	0.88 ± 0.02		0.95
299	0.89 ± 0.02		0.95
300	0.89 ± 0.02		0.95
301	0.90 ± 0.01	0.88 ± 0.01	0.95
302	0.90 ± 0.01	0.85 ± 0.02	0.95
303	0.90 ± 0.01	0.87 ± 0.09	0.95
304	0.89 ± 0.01	0.88 ± 0.09	0.95
305	0.90 ± 0.01	0.89 ± 0.10	0.95
306	0.88 ± 0.01	0.85 ± 0.07	0.91
307	0.84 ± 0.01	0.85 ± 0.10	0.85
308	0.79	0.79 ± 0.02	0.74

[a] Photolysis wavelength. [b] Determined from the PHOFEX spectrum for $O(^3P)$ measured in this study, by using 0.79 at 308 nm as a reference value (see text). Uncertainties of the values at 297−307 nm do not include that of the reference value. [c] Taken from ref 22. It has been reported that the $O(^1D)$ yield value is 0.89 ± 0.02 between 289 and 305 nm, almost independent of temperature (203−320 K). [d] NASA/JPL recommendation for atmospheric modeling (ref 27).

et al. [7] are used as $\sigma_{abs}(\lambda)$. The PHOFEX spectrum for $O(^3P)$ at 295 K in Figure 2 is proportional to the partial cross-section spectrum, that is $\sigma_{3P}(\lambda) = s_{3P}Y_{3P}(\lambda)$. Since the vertical scale of the $O(^3P)$ PHOFEX spectrum in Figure 3 is not absolute but relative, the value of coefficient s_{3P} is determined so that the values of the $O(^1D)$ yield at 308 nm is 0.79. Several studies have indicated that the absolute $O(^1D)$ quantum yield is 0.79.[21,22,35,36] Our $O(^1D)$ quantum yields shown in Figure 5 were thus obtained in the photolysis wavelength range 297−314 nm. Table 2 lists the $O(^1D)$ quantum yield values from O_3 photolysis at room temperature. The uncertainties of the $O(^1D)$ quantum yields listed in Table 2 come from the run-by-run fluctuations in the $O(^3P)$ PHOFEX spectrum measurements.

Discussion

A. Photodissociation Processes of O_3 around the Threshold into $O(^1D) + O_2(a^1\Delta_g)$. The cutoff wavelength in the $O(^1D)$ PHOFEX spectrum of jet-cooled O_3 (Figure 3) corresponds to the energetic threshold into channel (1). The threshold energy of channel (1) has been measured to be 309.44 ± 0.03 nm.[26] The quantum yield spectrum for $O(^1D)$ production from O_3 photolysis in Figure 5 indicates a marked falloff at $\lambda \approx 306$ nm. Many studies on the $O(^1D)$ quantum yield have shown that the $O(^1D)$ quantum yield starts to decline at $\lambda \approx 306$ nm.[1−3,18,20−23] It has been thought that the decrease of the $O(^1D)$ quantum yield toward the longer photolysis wavelength should be due to the thermochemical threshold for formation of $O(^1D)$ via channel (1). However, the exact threshold wavelength for it has been measured to be 309.44 ± 0.03 nm.[26] Therefore, the wavelength of 306 nm where the marked falloff is observed in the $O(^1D)$ quantum yield spectrum is shorter than that of the exact channel (1) threshold. There has been no explanation about the "early decrease" of the $O(^1D)$ formation at wavelengths shorter than the exact threshold. Photolysis of the internally excited O_3 molecules cannot explain the early decrease of the $O(^1D)$ formation at wavelengths shorter than the threshold, although it can explain the formation of $O(^1D)$ at wavelengths longer than the threshold.[15−23,28]

The sum of quantum yields for $O(^3P)$ and $O(^1D)$ must be unity at wavelengths $\lambda > 237$ nm, in wihich the wavelength is the thermochemical threshold for channel of $O(^1S) + O_2(X^3\Sigma_g^-)^3$. The jet-cooled PHOFEX spectrum for $O(^1D)$ shows the clear-cut-off at the channel (1) threshold of 309.44 nm, as shown in Figure 3. At the wavelengths longer than the threshold of 309.44 nm, photoexcited O_3 molecules mainly dissociate into channel (2) by changing the surface from the photoprepared $^1B_2$ state to the R state (see Figure 1). When the photon energy exceeds the channel (1) threshold, the direct dissociation path to $O(^1D) + O_2(a^1\Delta_g)$ is opened in the photoexcited state. Therefore, a sudden decrease of the $O(^3P)$ formation yield is expected at the channel (1) threshold, since the direct dissociation to the $O(^1D) + O_2(a^1\Delta_g)$ products should be more efficient than the potential switching to form the $O(^3P) + O_2(X^3\Sigma_g^-)$ products. However, the PHOFEX spectra for $O(^3P)$ atoms under 295 K and jet-cooled conditions does not show such a sudden decrease at the shorter wavelength side of the threshold. Both of the $O(^3P)$ PHOFEX spectra show gradual decrease from the threshold (309.44 nm) toward the shorter wavelength and then have minima around 306 nm, as shown in Figure 3. The considerable formation of $O(^3P)$ atoms between 306 and 309.44 nm in Figure 3 is responsible for the early decrease of the $O(^1D)$ quantum yield spectrum shown in Figure 5. The product branching between the $O(^1D)$ and $O(^3P)$ atoms is decided by the dissociation rates to each product. The early decrease in the $O(^1D)$ quantum yield spectrum between 306 and 309.44 nm indicates that the dissociation rate to $O(^1D) + O_2(a^1\Delta_g)$ [channel (1)] at those wavelengths is suppressed and/or that the dissociation rate to $O(^3P) + O_2(X^3\Sigma_g^-)$ [channel (3)] is enhanced.

The early decrease in the $O(^1D)$ quantum yield spectrum can be interpreted by the presence of an exit barrier on the $^1B_2$ photoexcited-state surface along the bond breaking coordinate into $O(^1D) + O_2(a^1\Delta_g)$. The exit barrier can reduce the rate of direct dissociation of $O_3(^1B_2)$ into $O(^1D) + O_2(a^1\Delta_g)$, when the excitation energy is below the barrier top. Existence of the exit barrier has also been suggested by theoretical calculations.[10−13,37] The $O(^1D)$ PHOFEX spectrum measured under jet-cooled conditions shown in Figure 3 supports the existence of the barrier. The jet-cooled PHOFEX spectrum for $O(^1D)$ shows sharp structure in the range $306 < \lambda < 309.44$ nm, while it exhibits broad features at $\lambda < 306$ nm. The broad features at $\lambda < 306$ nm may be attributed to the bound-free transition, that

is, O_3 molecules are excited to the repulsive part of the $^1B_2$ state above the barrier top. They dissociate predominantly into $O(^1D) + O_2(a^1\Delta_g)$ quickly. On the other hand, the sharp structure in the jet-cooled PHOFEX spectrum for $O(^1D)$ in the range $306 < \lambda < 309.44$ nm is caused by long lifetimes in the upper state. This is due to the transitions onto quasi-bound states below the exit barrier top in the $^1B_2$ surface. The line widths (fwhm) of the peaks in this wavelength range in the jet-cooled PHOFEX spectrum of $O(^1D)$ (Figure 4) are in the range $7-35$ cm^{-1}, which correspond to the lifetimes of $0.2-0.8$ ps. The sharpest peak observed at 309.1 nm has the line width of 7 cm^{-1} in fwhm, the value of which is as small as the rotational broadenings of the structural peaks in the jet-cooled PHOFEX spectrum for $O(^1D)$ generated from the Huggins band photolysis of O_3 at $321 < \lambda < 328$ nm which is below the threshold to $O(^1D) + O_2(a^1\Delta_g)$ under jet-cooled conditions.[15]

The formation of $O(^1D)$ atoms is still observed even when the O_3 molecule is excited to the quasi-bound state below the exit barrier on the $^1B_2$ PES between 306 and 309.44 nm. The O_3 molecule in the quasi-bound levels in the $^1B_2$ state may change its potential surface to another electronic state surface which leads to $O(^1D) + O_2(a^1\Delta_g)$ fragmentation without any barrier in the exit channel, and also change surfaces to the R surface which leads to $O(^3P) + O_2(X^3\Sigma_g^-)$ fragmentation (see Figure 1). There are nine states correlating to channel (1) other than the $^1B_2$ state. However, the studies about them have been well performed neither theoretically nor experimentally. The rates of the crossings from the $^1B_2$ state to the two different states compete with each other in the quasi-bound states below the barrier. The barrier height is estimated to be about 400 cm^{-1} from the energy difference between 306 and 309.44 nm. Theoretical studies on the $O_3(^1B_2)$ PES also predicted the exit barrier to the $O(^1D) + O_2(a^1\Delta_g)$ products. Leforestier et al.[36] carried out the *ab-initio* calculations for the $O_3(^1B_2)$ PES and showed that the surface has the exit barrier along the $O-O_2$ bond breaking coordinate. The barrier height from the dissociation limit into $O(^1D) + O_2(a^1\Delta_g)$ was calculated to be about 1550 cm^{-1}. The value predicted theoretically is larger than that reported here.

In the wavelength region of $\lambda < 306$ nm, it is interesting that the spectral features of the two jet-cooled PHOFEX spectra for $O(^1D)$ and $O(^3P)$ are different from each other (see Figure 3). The $O(^1D)$ PHOFEX spectrum has broad features in this wavelength region, while the $O(^3P)$ PHOFEX spectrum shows sharp peaks with high aspect ratios. This fact suggests that the upper electronic states leading to the channel (2) products have longer lifetimes than those to the channel (1) products. The initially photoprepared upper electronic states which is responsible for the both product pairs should be on the same $^1B_2$ surface. The states on the $^1B_2$ surface, which have longer lifetimes and more chances to cross the seam with the R surface, appears in the $O(^3P)$ PHOFEX spectrum as sharp structure. On the other hand, the states which have relatively shorter lifetimes dissociating into $O(^1D) + O_2(a^1\Delta_g)$ are reflected in the $O(^1D)$ PHOFEX spectrum as the broad features. Detailed analysis of the vibrational structure in the jet-cooled $O(^3P)$ PHOFEX above the threshold wavelength will be presented in a future paper.

B. $O(^1D)$ Quantum Yield in the Range $\lambda = 297-308$ nm. Figure 5 shows the quantum yield of the $O(^1D)$ formation from the UV photolysis of O_3 at 295 K, as a function of the photolysis wavelength, which are obtained from the $O(^3P)$ PHOFEX spectrum shown in Figure 2. In this study, the absolute values of the $O(^1D)$ quantum yield are determined by referring the value of 0.79 at 308 nm, as mentioned in the results. The quantum yield spectrum between 305 and 316 nm coincides with that of the absolute measurements by Takahashi et al.[21] They obtained the absolute $O(^1D)$ quantum yield between 305 and 328 nm by adjusting the sensitivity factors, s_{3P} and s_{1D}, so that the sum of the PHOFEX spectra for $O(^3P)$ and $O(^1D)$, that is $Y_{3P}(\lambda)$ and $Y_{1D}(\lambda)$, fitted to the total absorption spectrum of O_3, $\sigma_{abs}(\lambda)$:

$$\sigma_{abs}(\lambda) \equiv \sigma_{1D}(\lambda) + \sigma_{3P}(\lambda) = s_{3P}Y_{3P}(\lambda) + s_{1D}Y_{1D}(\lambda) \quad (8)$$

In the eq 8, $\sigma_{1D}(\lambda)$ and $\sigma_{3P}(\lambda)$ are the partial cross sections for producing $O(^1D)$ and $O(^3P)$ fragments, respectively. From the measurements, they reported the absolute value of the $O(^1D)$ quantum yield to be 0.79 ± 0.12 at 308 nm. Greenblatt and Wiesenfeld[35] reported the value of 0.79 ± 0.02 for the $O(^1D)$ quantum yield from the 308 nm photolysis of O_3 at 298 K. Talukdar et al.[22] reported the value of 0.79 ± 0.10 at 298 K. Another study by Talukdar et al.[36] reported the value of 0.78 ± 0.02 at 298 K. In these studies[21,35,36] the time profile of the resonance fluorescence intensity for the $O(^3P)$ products was measured by using a microwave-powered Oxygen atom lamp. The time profile was characterized by a rapid initial jump followed by a slower increase. The rapid rise is due to the direct production of $O(^3P)$, while the slower increase is to the indirect formation from the $O(^1D)$ deactivation. By analyzing the profile, the absolute quantum yields of $O(^1D)$ were obtained. The results at 308 nm from the resonance lamp experiments are in excellent agreement with that from the PHOFEX spectra measurements by Takahashi et al.[21] In Figure 5, the $O(^1D)$ quantum yield from the UV photolysis of O_3 recommended by NASA/JPL[27] and the experimental results measured by Talukdar et al.[22] are also plotted for comparison. It should be noted that the $O(^1D)$ quantum yield between 297 and 305 nm obtained from the present study is almost independent of the wavelength and is $\sim$0.89 (Table 2). Our results are in excellent agreement with the recent measurements by Talukdar et al.[22] in which they reported the $O(^1D)$ quantum yield between 289 and 305 nm is 0.89 ± 0.02. On the other hand, the NASA/JPL recommendation[27] is 0.95 in this photolysis wavelength range.

In the wavelength range $\lambda < 308$ nm, the PHOFEX spectrum of $O(^3P)$ reflects the change of the $O(^1D)$ quantum yield more clearly than that of $O(^1D)$, since the $O(^1D)$ quantum yields are close to unity. Figure 2 shows the PHOFEX spectrum for $O(^3P)$ at 295 K. The dotted curve drawn in Figure 2 indicates a hypothetical spectrum of the $O(^3P)$ PHOFEX, based on the assumption that the $O(^1D)$ quantum yield increases from the value of 0.79 to 0.95 with decreasing the photolysis wavelength from 308 to 305 nm as recommended by NASA/JPL. The large difference between the actual and hypothetical spectra clearly suggests that the $O(^1D)$ quantum yield is not as high as 0.95 at 305 nm. The $O(^3P)$ PHOFEX spectrum between 297 and 305 nm shown in Figure 2 is almost proportional to the absorption spectrum. This results in the almost constant behavior in the $O(^1D)$ quantum yield spectrum between 297 and 305 nm ($\sim$0.89), as shown in Figure 5.

C. Model Calculations for $O(^1D)$ Production from the O_3 Photolysis. Figure 6 shows the schematic diagram which indicates the contribution of the various photodissociation processes to the quantum yield spectrum for $O(^1D)$ atoms produced from O_3 photolysis in the wavelength range 305−329 nm. This diagram is taken from the paper presented by Takahashi et al.[21] In Figure 6, the region I indicates the contribution of the hot band excitation followed by dissociation via channel (1) at 295 K. Takahashi et al.[21] pointed out that the

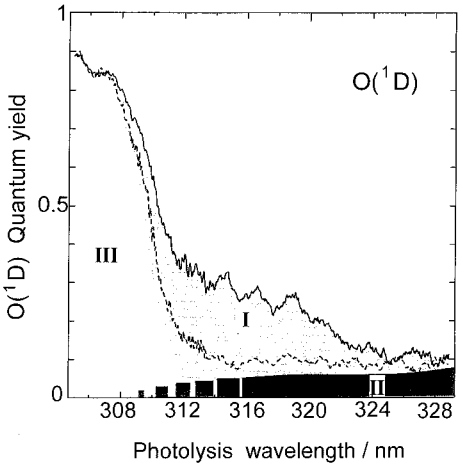

Figure 6. Schematic diagram depicting the contributions made by the various dissociation processes contributing to the quantum yield spectra for $O(^1D)$ atoms from O_3 photolysis in the wavelength range 305−328 nm. This figure is taken from ref 21. The solid curve is the quantum yield spectrum obtained experimentally at 295 K, while the dashed curve is that obtained at 227 K. Region I (shaded) indicates the contribution from the hot band excitation leading to $O(^1D) + O_2(a^1\Delta_g)$ [channel (1)] at 295 K. Region II (black) represents the contribution from the spin-forbidden process leading to $O(^1D) + O_2(X^3\Sigma_g^-)$ [channel (2)]. Region III corresponds to the $O(^1D)$ formation following excitation of vibrationless parent molecules and dissociation to $O(^1D) + O_2(a^1\Delta_g)$ [channel (1)].

asymmetric stretching vibration in the electronic ground state was most efficient in promoting the fragmentation into channel (1). The predominant contribution of the antisymmetric stretching vibration to the hot band excitation has been explained by large enhancement of the Franck−Condon factors between the photoexcited state and the vibrationally excited level in the ground electronic state. The region II in Figure 6 depicts the contribution of the $O(^1D)$ formation via spin-forbidden channel (3), which is almost independent of the O_3 temperature. Takahashi et al.[21] suggested that the relative contribution from channel (3) to the $O(^1D)$ quantum yield decreases from the value of 0.08 at 328 nm toward the shorter wavelength. The region III in Figure 6 depicts the $O(^1D)$ formation via channel (1) following excitation of O_3 molecules in their ground vibrational level.

To verify the above-mentioned mechanism for $O(^1D)$ formation, we present a quantitative model which accounts for the wavelength and temperature dependence of the $O(^1D)$ quantum yield in the photolysis of O_3, $\Phi_{1D}(\lambda,T)$, based on the $O(^1D)$ PHOFEX spectrum obtained in this study under the jet-cooled conditions. Model calculations for $\Phi_{1D}(\lambda,T)$ have also been proposed by Adler-Golden et al.[38] and Michelsen et al.[28] In our new model, recent findings such as observation of the spin-forbidden channel (3) and propensity of the antisymmetric vibration in the hot band excitation, are taken into account.

The partial cross section to produce $O(^1D)$ atoms from O_3 photolysis, σ_{1D}, should be the summation of cross sections for each process I, II, and III, as depicted in Figure 6

$$\sigma_{1D}(E_{ph},T) = \sigma_{1D}{}^{I}(E_{ph},T) + \sigma_{1D}{}^{II}(E_{ph},T) + \sigma_{1D}{}^{III}(E_{ph},T) \quad (9)$$

In eq 9, σ_{1D} is given as a function of photon energy, E_{ph}, and gas temperature, T. The jet-cooled $O(^1D)$ PHOFEX spectrum obtained in the present study (Figure 3) should be very close to the PHOFEX spectrum at $T_{rot} = 0$ K, that is, $\sigma_{1D}{}^{III}(E_{ph},T=0)$. This is because that in the present experiments the rotational temperature of parent O_3 molecules is as low as 3 K and the vibrational temperature is also low in the supersonic beam conditions.[34] Since the vertical scale of the $O(^1D)$ PHOFEX spectrum in Figure 3 is relative, the absolute scale is given by multiplying a sensitivity factor to the spectrum measured

$$\sigma_{1D}{}^{III}(E_{ph},T=0) = s_{1D}Y_{1D}(E_{ph},T=0) \quad (10)$$

where $Y_{1D}(E_{ph},T=0)$ is the jet-cooled PHOFEX spectrum for $O(^1D)$ shown in Figure 3.

Next, we calculate the hot-band cross sections, $\sigma_{1D}{}^{I}(E_{ph},T)$, from the $\sigma_{1D}{}^{III}(E_{ph},T=0)$ derived above. The rotational and vibrational energies in a parent O_3 molecule are assumed to be equivalent to the increase of the photolysis photon energy. The contribution of the $O(^1D)$ production from the rotationally excited but vibrationally cold O_3, $\sigma_{1D}{}^{III}(E_{ph},T)$, is calculated by convoluting the cross section $\sigma_{1D}{}^{III}(E_{ph},T=0)$ with the rotational distribution function, P_{rot}

$$\sigma_{1D}{}^{III}(E_{ph},T) = \sum_{E_{rot}} \sigma_{1D}{}^{III}(E_{ph} + \alpha_{rot}E_{rot},T=0)\, P_{rot}(E_{rot},T) \quad (11)$$

where E_{rot} is the rotational energy of the parent O_3 and α_{rot} is the fraction of rotational energy which is effective in overcoming the energy threshold for channel (1). The physical quantity of α_{rot} is restricted to the range 0−1.[39] For P_{rot} the normalized classical expression is assumed,

$$P_{rot}(E_{rot},T) = (E_{rot})^{1/2}\, T^{-3/2} \exp\left(-\frac{E_{rot}}{kT}\right) \quad (12)$$

where k is the Boltzmann constant. E_{rot} is rotational energy of parent O_3. Then, the effects of vibrational excitation in the hot-band cross sections are included by taking the vibrational energies, vibrational distribution function, and Franck−Condon factors into account:

$$\sigma_{1D}{}^{I}(E_{ph},T) = \sum_{E_{vib}} f_{v''}\sigma_{1D}{}^{III}(E_{ph}+E_{vib},T)\, P_{vib}(E_{vib},T) \quad (13)$$

where $f_{v''}$ is a ratio of the Franck−Condon factors between vibrationally hot and cold band excitations, $FCF(v'')/FCF(v''=0)$. The ratios $f_{v''}$ are given as linear functions of E_{ph}. The $P_{vib}(E_{vib},T)$ is the vibrational distribution function at a temperature T, which is given by the Boltzmann function. E_{vib} is vibrational energy of parent O_3. Since the contribution of antisymmetric vibration is predominant in the hot band excitation, the vibrational levels of $v'' = 1$ ($E_{vib} = 1042$ cm^{-1}) and $v'' = 2$ ($E_{vib} = 2084$ cm^{-1}) are taken into account. The fundamental frequency of the antisymmetric vibration of O_3 in the electronic ground state was taken from the paper by Barbe et al.[40] The contributions of $v'' \geq 3$ are ignored because of the small populations in the vibrational levels even at room temperatures. Consequently, we obtain the partial cross sections for region I in Figure 6, $\sigma_{1D}{}^{I}(E_{ph},T)$.

Figure 7a is the result of the present model calculations giving the partial cross sections in arbitrary units for $O(^1D)$ formation in the photolysis of O_3 between 305 and 329 nm. The solid line in Figure 7a indicates the partial cross sections for rotationless ($T_{rot} = 0$ K) and vibrationless ($v'' = 0$) O_3 molecule in arbitrary units, that is, $Y_{1D}{}^{III}(E_{ph},T=0)$. The dotted line represents the cross sections for $O(^1D)$ formation from the rotationally excited and vibrationally cold O_3 molecules, which is the result of the convolution of the rotational excitation function at room temperature (eq 12) to the cross sections from rotationally and vibrationally cold O_3 molecules. The broken

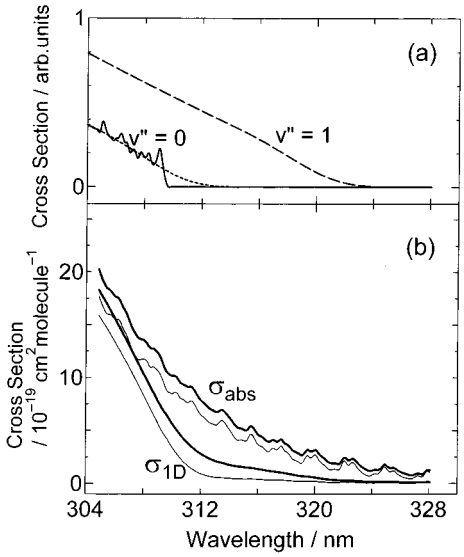

Figure 7. (a) Cross sections for $O(^1D)$ formation from the photolysis of O_3, which are obtained by the physical model calculations in this study (see text).The solid line is the yield spectrum of the $O(^1D)$ formation following the photoexcitation of the vibrationless ($v'' = 0$) and rotationless ($T_{rot} = 0$) O_3 molecules, which is assumed to be proportional to the jet-cooled $O(^1D)$ PHOFEX spectrum shown in Figure 3. The dotted line is the $O(^1D)$ yield spectrum calculated for the $v'' = 0$ state of O_3 with thermal rotational excitation at 295 K. The broken line is the yield spectrum simulated for the $v'' = 1$ state of O_3 with $T_{rot} = 295$ K. (b) Partial absorption cross section spectra (σ_{1D}) for the $O(^1D)$ formation from the O_3 photolysis at 295 K (thick line) and 228 K (thin line), which are calculated from the spectra shown in (a) using the fitting parameters listed Table 3. Total absorption cross section spectra (σ_{abs}) measured by Malicet et al.[7] are also shown at 295 K (thick line) and 228 K (thin line).

line is the hot-band partial cross sections calculated for O_3 molecules with $v'' = 1$ and $T_{rot} = 295$ K.

The partial cross sections for the $O(^1D)$ production via the spin-forbidden channel (3), $\sigma_{1D}^{II}(E_{ph},T)$, which is depicted as region II in Figure 6, are calculated. Experimental studies showed that the $O(^1D)$ formation via channel (3), Φ_{1D}^{II}, gradually decreases from the value of 0.08 at 328 nm toward the shorter photolysis wavelength. The region II cross sections in the model calculations are thus given by multiplying the total O_3 absorption by the region II $O(^1D)$ quantum yield Φ_{1D}^{II} reported in the experimental study of Takahashi et al.[21] Excitation energy dependent values for Φ_{1D}^{II} in the model calculations are given by the linear function so that it is to be 0.08 at 329 nm and it decreases toward the shorter photolysis wavelength. The effect of the temperature on the region II cross sections $\sigma_{1D}^{II}(E_{ph},T)$ is neglected in the model calculations, since the region II $O(^1D)$ quantum yield Φ_{1D}^{II} has been found to be almost independent of the temperature by several experimental studies.[20−22]

As a result, we obtain the partial cross sections for $O(^1D)$ production, $\sigma_{1D}(E_{ph},T)$ in eq 9. The parameters used in the model calculations are summarized in Table 3. Figure 7b shows the resultant $O(^1D)$ cross sections which are calculated with this model for 295 (thick line) and 227 K (thin line). The absorption cross sections for parent O_3 at 295 and 228 K [7] are also plotted for comparison, by thick and thin lines, respectively. Applying the modeled cross sections of $\sigma_{1D}(E_{ph},T)$ to eq 7, we can derive the wavelength and temperature dependent quantum yield of the $O(^1D)$ production in the O_3 photolysis. Figure 8 shows the comparison of the model calculation results with the experimental results presented by Takahashi et al.[21] The model calculations well reproduce the experimental results for the

TABLE 3: Parameters Used in Our Physical Model Calculations for the Wavelength and Temperature Dependent Quantum Yield for $O(^1D)$ Production from the Ultraviolet Photolysis of O_3 in the Wavelength Range 305−329 nm

parameter	value
E_{th}[a]	32316 cm^{-1} (=309.44 nm)
$f_{v''=1}$[b]	2 at 33 333 cm^{-1} (=300 nm) and 12 ± 2 at 30 395 cm^{-1} (=329 nm), with the linear dependence on E_{ph}
$f_{v''=2}$[c]	60 ± 20
α_{rot}[d]	0.65 ± 0.1
σ_{1D}^{II}[e]	$\sigma_{abs}\Phi_{1D}^{SF}$, where Φ_{1D}^{SF} is 0.08 at 30 395 cm^{-1} (=329 nm) and 0.02 at 32 316 cm^{-1} (=309.44 nm), with the linear dependence on E_{ph}

[a] Threshold energy dissociating into $O(^1D) + O_2(a^1\Delta_g)$, which corresponds to the wavelength of 309.44 nm (ref 26). This value was fixed in the model calculations. [b] Ratio of Franck−Condon factors, FCF(v''=1)/FCF(v''=0), of the optical transitions from the vibrationless and the vibrationally excited levels in the ground electronic state, which was given by the linear function so that they are to be 2 and 12 ± 2 at 33 333 cm^{-1} (=300 nm) and 30 395 cm^{-1} (=329 nm) (see text). [c] Same as b, but for FCF(v''=2)/FCF(v''=0). Given by the constant. [d] Fraction of rotational energy effective in overcoming the threshold into the $O(^1D) + O_2(a^1\Delta_g)$ products (see text). [e] The partial cross sections for forming $O(^1D)$ atoms via the spin-forbidden $O(^1D) + O_2(^3\Sigma_g^-)$ channel, which were obtained by multiplying the O_3 absorption by the photolysis energy dependent $O(^1D)$ quantum yield (see text). The $O(^1D)$ quantum yield was given by the linear function so that it is to be 0.08 at 30 395 cm^{-1} (=329 nm) and to be 0.02 at 32 316 cm^{-1} (=309.44 nm).

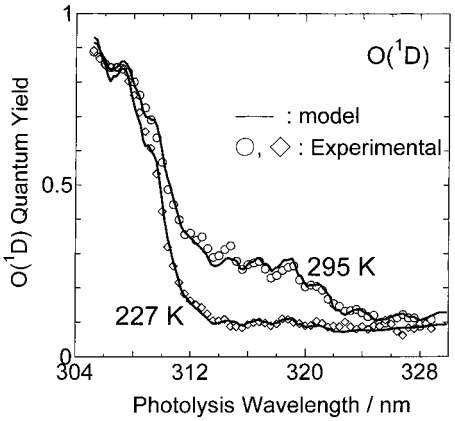

Figure 8. Quantum yields of the $O(^1D)$ formation from the UV photolysis of O_3 at 295 and 227 K as functions of the photolysis wavelength. Solid lines are the results of the model calculations. Open circles and rhombuses are experimental results at 295 and 227 K, respectively, which are reported by Takahashi et al.[21]

$O(^1D)$ quantum yield values over the 305−329 nm range both at 227 and 295 K. The results of the present model calculations quantitatively confirm the mechanisms for the $O(^1D)$ formation processes (Figure 6) suggested from the experimental studies by Takahashi et al.[21]

Conclusion

The PHOFEX spectra for both $O(^1D)$ and $O(^3P)$ fragments produced from the photodissociation of O_3 in the wavelength range 296−316 nm are measured under jet-cooled and room-temperature conditions. The PHOFEX spectra for $O(^3P)$ taken under jet-cooled and room temperature conditions do not suddenly decrease even at the wavelengths shorter than the thermodynamic threshold wavelength of the $O(^1D) + O_2(a^1\Delta_g)$ dissociation at 309.44 nm. This suggests the presence of the exit barrier along the $O-O_2$ dissociation coordinate in the $^1B_2$ photoexcited electronic state of O_3. The sharp peaks are observed

in both PHOFEX spectra for $O(^1D)$ and $O(^3P)$, which may be attributable to the long lifetimes of the quasi-bound levels between the thermodynamic threshold and the barrier top. The PHOFEX spectrum for $O(^3P)$ at 295 K provides the accurate $O(^1D)$ quantum yield values between 297 and 316 nm. The $O(^1D)$ quantum yields between 297 and 305 nm are almost constant and obtained to be about 0.89. This value is in good agreement with the recent report by Talukdar et al.[22] and is smaller than the NASA/JPL recommendation.[27] The quantitative model calculations for the $O(^1D)$ formation are presented to explain the temperature and wavelength dependence of the $O(^1D)$ quantum yield between 305 and 329 nm, which is based on the dissociation mechanisms presented by Takahashi et al.[21] The model includes the contributions of the spin-forbidden process (channel (3)) and thermal excitation in the vibrational and rotational states of O_3 molecules in the electronically ground state. The results of the model calculation well reproduce the $O(^1D)$ quantum yields obtained experimentally.

Acknowledgment. Support of this work by Grants-in-Aid from the Ministry of Education, Science and Culture, is acknowledged. This work was partly supported by the research project, "computational chemistry for atmospheric environmental molecule" under Research and Development Applying Advance Computational Science and Technology administrated by Japan Science and Technology Corporation (ACT-JST).

References and Notes

(1) Brasseur, G. P.; Orlando, J. J.; Tyndall, G. S. *Atmospheric Chemistry and Global Change*; Oxford University Press: New York, 1999.

(2) Finlayson-Pitts, B. J.; Pitts. Jr. J. N. *Chemistry of the Upper and Lower Atmosphere, Theory, Experiments, and Applications*; Academic Press: California, 1999.

(3) Atkinson, R.; Baulch, D. L.; Cox, R. A.; Hampson, R. F., Jr.; Kerr, J. A.; Rossi, M. J.; Troe, J. *J. Phys. Chem. Ref. Data*. **1997**, *26*, 1329.

(4) Freeman, D. E.; Yoshino, K.; Esmond, J. R.; Parkinson, W. H. *Planet. Space Sci*. **1984**, *32*, 248.

(5) Molina, L. T.; Molina, M. J. *J. Geophys. Res.* **1986**, *91*, 14501.

(6) Yoshino, K.; Esmond, J. R.; Freeman, D. E.; Malicet, J. *J. Atmos. Chem.* **1992**, *15*, 145.

(7) Malicet, J.; Daumont, D.; Charbonnier, J.; Parisse, C.; Chakir, A.; Brion, J. *J. Atmos. Chem.* **1995**, *21*, 263.

(8) Hay, P. J.; Pack, R. T.; Walker, R. B.; Heller, E. J. *J. Phys. Chem.* **1982**, *86*, 862.

(9) Sinha, A.; Imre, D.; Goble, J. H., Jr.; Kinsey, J. L. *J. Chem. Phys.* **1986**, *84*, 6108.

(10) LeQuéré, F.; Leforestier, C. *Chem. Phys. Lett.* **1992**, *189*, 537.

(11) Bludsky, O.; Jensen, P. *Mol. Phys.* **1997**, *91*, 653.

(12) Banichevich, A.; Peyerimhoff, S. D.; Green, F. *Chem. Phys.* **1993**, *178*, 155.

(13) Banichevich, A.; Peyerimhoff, S. D. *Chem. Phys.* **1993**, *174*, 93.

(14) Jones, J. A. *J. Chem. Phys.* **1994**, *100*, 3407.

(15) Takahashi, K.; Kishigami, M.; Taniguchi, N.; Matsumi, Y.; Kawasaki, M. *J. Chem. Phys.* **1997**, *106*, 6390.

(16) Takahashi, K.; Matsumi, Y.; Kawasaki, M. *J. Phys. Chem.* **1996**, *100*, 4084.

(17) Takahashi, K.; Kishigami, M.; Matsumi, Y.; Kawasaki, M.; Orr-Ewing, A. J. *J. Chem. Phys.* **1996**, *105*, 5290.

(18) Ball, S. M.; Hancock, G.; Martin, S. E.; Pinot de Moira, J. C. *Chem. Phys. Lett.* **1997**, *264*, 531.

(19) Denzer, W.; Hancock, G.; Pinot de Moira, J. C.; Tyley, P. L. *Chem. Phys. Lett.* **1997**, *280*, 496; *Chem. Phys.* **1998**, *231*, 109.

(20) Silvente, E.; Richter, R. C.; Zheng, M.; Saltzman, E. S.; Hynes, A. J. *Chem. Phys. Lett.* **1997**, *264*, 309. Bauer, D.; D'Ottone, L.; Hynes, A. J. *Phys. Chem. Chem. Phys.* **2000**, *2*, 1421.

(21) Takahashi, K.; Taniguchi, N.; Matsumi, Y.; Kawasaki, M.; Ashfold, N. M. R. *J. Chem. Phys.* **1998**, *108*, 7161.

(22) Talukdar, R. K.; Longfellow, C. A.; Gilles, M. K.; Ravishankara, A. R. *Geophys. Res. Lett.* **1998**, *25*, 143.

(23) Ravishankara, A. R.; Hancock, G.; Kawasaki, M.; Matsumi, Y. *Science* **1998**, *280*, 60.

(24) O'Keeffe, P.; Ridley, T.; Wang, S.; Lawley, K. P.; Donovan, R. J. *Chem. Phys. Lett.* **1998**, *298*, 368.

(25) O'Keeffe, P. Ridley, T.; Lawley, K. P.; Maier, R. R. J.; Donovan, R. J. *J. Chem. Phys.* **1999**, *110*, 10803.

(26) Taniguchi, N.; Takahashi, K.; Matsumi, Y.; Dylewski, S. M.; Geiser, J. D.; Houston, P. L. *J. Chem. Phys.* **1999**, *111*, 10803.

(27) DeMore, W. P.; Sander, S. P.; Golden, D. M.; Hampson, R. F.; Kurylo, M. J.; Howard, C. J.; Ravishankara, A. R.; Kolb, C. E.; Molina, M. J. *Chemical Kinetics and Photochemical Data for Use in Stratospheric Modeling*; Evaluation Number 12, JPL Publication 97-4; Jet Propulsion Laboratory, California Institute of Technology, Pasadena, CA, 1997.

(28) Michelsen, H. A.; Salawitch, R. J.; Wennberg, P. O.; Anderson, J. G. *Geophys. Res. Lett.* **1994**, *21*, 2227.

(29) Gerstenkorn, S.; Luc, P. *Atlas du Spectre D'Absorption de la Molecule D'Iode*; CNRS: Paris, 1978.

(30) Hilber, G.; Lago, A.; Wallenstein, R. *J. Opt. Soc. Am.* **1987**, *B4*, 1753.

(31) Hilbig, R.; Wallenstein, R. *Appl. Opt.* **1982**, *21*, 913.

(32) Shamusuddin, S. M.; Inagaki, Y.; Matsumi, Y.; Kawasaki, M. *Can. J. Chem.* **1993**, *72*, 637.

(33) Rottke, H.; Zacharias, H. *Opt. Commun.* **1985**, *55*, 87.

(34) Scoles, G. *Atomic and Molecular Beam Methods*; Oxford University Press: New York, 1988; Vol. 1.

(35) Greenblatt, G. D.; Wiesenfeld, J. R. *J. Chem. Phys.* **1983**, *78*, 4924.

(36) Talukdar, R. K.; Gilles, M. K.; Battin-Leclerc, F.; Ravishankara, A. R.; Fracheboud, J.-M.; Orlando, J. J.; Tyndall, G. S. *Geophys. Res. Lett.* **1997**, *24*, 1091.

(37) Leforestier, C.; L*e*Quéré, F.; Yamashita, K.; Morokuma, K. *J. Chem. Phys.* **1994**, *101*, 3806.

(38) Alder-Golden, S. M.; Schweitzer, E. L.;. Steinfeld, J. L. *J. Chem. Phys.* **1982**, *76*, 2201.

(39) Johnston, H. S.; Davis, H. F.; Lee, Y. T. *J. Phys. Chem.* **1996**, *100*, 4713.

(40) Barbe, A.; Secroun, C.; Jouve, P. *J. Mol. Spectosc.* **1974**, *49*, 171.